Applied Catalysis B: Environmental 236 (2018) 368–376

Contents lists available at ScienceDirect

Applied Catalysis B: Environmental

journal homepage: www.elsevier.com/locate/apcatb

Dehydrochlorination of 1, 1, 2-trichloroethane over SiO_2-supported alkali and transition metal catalysts: Tunable selectivity controlled by the acid - base properties of the catalysts

Tong-Yang Song[a], Zhao-Xia Dong[a], Jian-Dong Song[a], Xiao-Xia Wang[a], Guan-Qun Xie[a,b,*], Meng-Fei Luo[a,b], Ji-Qing Lu[a,*]

[a]Key Laboratory of the Ministry of Education for Advanced Catalysis Materials, Institute of Physical Chemistry, Zhejiang Normal University, Jinhua, 321004, China
[b]Hangzhou Institute of Advanced Studies, Zhejiang Normal University, Hangzhou, 311231, China

ARTICLE INFO

Keywords:
Dehydrochlorination
vinylidene chloride
1, 2-dichloroethene
basicity-acidity
reaction mechanism.

ABSTRACT

Dehydrochlorination of 1, 1, 2-trichloroethane was performed on SiO_2 supported alkali metal (Na. K, Cs) and transition metal (Mn, Ni, Zn) catalysts. The surface basicity or acidity of the catalyst exerted great influence on catalytic behaviors. The catalysts with higher amount of base or acid sites resulted in higher activity due to more adsorption sites for reactant. The basic catalysts (Cs/SiO_2 and K/SiO_2) tended to form vinylidene chloride with a selectivity up to 80 %; the neutral catalysts (Na/SiO_2 and SiO_2) tended to form 1, 2-dichloroethene with a selectivity up to about 80 %; the acidic catalysts (Zn/SiO_2, Mn/SiO_2 and Ni/SiO_2) tended to form 1, 2-dichloroethene with a selectivity up to 96 %. Proposed reaction mechanisms included an E1cb mechanism with a carbanion intermediate on the basic catalysts, an E2 concerted mechanism on the neutral catalysts, and an E1 mechanism with a carbonium intermediate on the acidic catalysts.

1. Introduction

Over the last few decades, it has been recognized that the direct emission of chlorinated hydrocarbons is detrimental to the environment (which causes acid rain, ozone layer depletion and greenhouse effects) and human health as most of them are carcinogenic [1,2]. Considering that such chlorinated hydrocarbons are produced in large quantity during various industrial processes, the treatment of such compounds becomes an important environmental and social problem. Comparing to direct incineration of such compounds [3], catalytic dehydrochlorination of chlorinated hydrocarbons to valuable chemicals is an environmentally-friendly approach [4]. 1, 1, 2-trichloroethane (TCE) is a typical chlorinated hydrocarbon, and the dehydrochlorination of TCE results in three main products (as shown in Scheme 1): 1, 1-dichloroethene (VDC) [5] and 1, 2-dichloroethene (1, 2-DCE) [6–8] which includes cis-1, 2-dicloroethene (cis-DCE) and trans-1, 2-dichloroethene (trans-DCE). VDC is the monomer of polyvinylidene chloride (PVDC), one famous green packaging material [9], cis-DCE has been widely used as solvents for paint, resin, wax, rubber and acetate fibers [10].

It was reported in early literature [11–13] that the acid-base properties of the catalyst could exert significant influence on the product selectivity during the TCE dehydrochlorination. It was reported that main product on solid base (CaO, SrO) catalysts was VDC, while that on the solid acid (such as silicon aluminum molecular sieves) was 1, 2-DCE. For example, Mochida and coworkers [14–18] found that high selectivity to VDC could be obtained over Al_2O_3, $CsCl/SiO_2$, $CsNO_3/SiO_2$ and KCl-B18/MB-3 A (dibenzo-18-crown-6-KCl) catalysts for the vapor phase catalytic dehydrochlorination of TCE. Tian et al. [19] reported a carbon nitride material with extra amino groups for efficient removal of HCl from TCE to VDC. Our previous work [20] supported pentaethylene hexamine (PEHA) on SiO_2 was found to be very high selective to VDC (up to 99%). In contrast, catalysts with surface acidity leads to the formation of 1, 2-DCE. For example, high selectivity to cis-DCE (82-91%) was obtained over $Mg(NO_3)_2/SiO_2$ and $Zn(NO_3)_2/SiO_2$ catalysts as reported in our previous works [10,21].

The above findings revealed that the distribution of the dehydrochlorination products is heavily dependent on the nature of the catalysts, and it is possible to control the selectivity to the desired products by turning the catalysts properties. Although it is clear that the acid/base properties of the catalysts are important for the formation of different products, deep study is needed to investigate the vital role of

* Corresponding authors at: Key Laboratory of the Ministry of Education for Advanced Catalysis Materials, Institute of Physical Chemistry, Zhejiang Normal University, Jinhua, 321004, China
E-mail addresses: gqxie@zjnu.cn (G.-Q. Xie), jiqinglu@zjnu.cn (J.-Q. Lu).

https://doi.org/10.1016/j.apcatb.2018.04.018
Received 2 January 2018; Received in revised form 9 April 2018; Accepted 12 April 2018
Available online 21 April 2018
0926-3373/

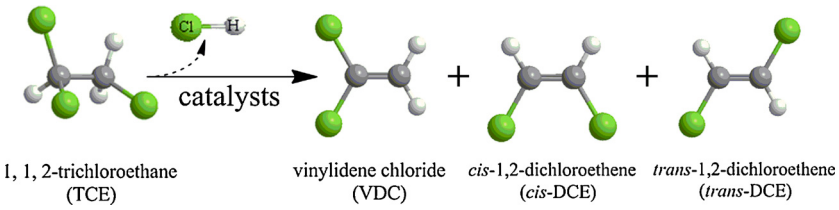

Scheme 1. Various products for dehydrochlorination of 1,1,2-trichloroethance.

such properties on the product distributions. For example, it is worthy of a systematic investigation to further understand how strength and type of acidity/basicity could control of selectivity. More importantly, the different product distributions on the base and acid catalysts may also be related to different reaction mechanisms, which needs to be clarified. Therefore, in this paper, two series of SiO_2 supported catalysts were prepared using MCl (M = Na, K, and Cs) and NCl_2 (N = Mn, Ni and Zn) as the precursors. The results vindicate the previous conclusions that the base catalysts lead to the formation of VDC while the acid catalysts lead to the formation of 1, 2-DCE. Moreover, it was found that the ratio of cis-DCE/trans-DCE was dependent on the type and strength of the acidic sites. Based on these results, possible reaction mechanisms were also proposed, which may provide some insights for the design of effective catalyst systems for dehydrochlorination of polychlorinated hydrocarbons.

2. Experimental

2.1. Catalyst preparation

The metal precursors used in this work included MCl (CsCl, KCl, NaCl, Sinopharm, 99 %), and NCl_2 ($ZnCl_2$, $MnCl_2{\cdot}4H_2O$ and $NiCl_2{\cdot}6H_2O$, Sinopharm, 98 %), which were purchased from commercial suppliers without further purification.

The SiO_2 supported metal chloride catalysts were prepared by an incipient wetness impregnation method, and the nominal contents of metal chlorides in all the catalysts were 4.8 mol.% (a M/Si molar ratio of 1/20). Taking the Cs/SiO_2 as an example, the catalyst was prepared as follows: 0.28 g of CsCl (1.66 mmol) was dissolved in deionized water, 2 g of SiO_2 support (33.3 mmol, S_{BET} = 378.8 $m^2\ g^{-1}$) was added. The mixture was sonicated for 30 min at room temperature, and kept for 6 h. Subsequently, the above mixture was mildly evaporated at 90 °C to remove water. The resulting solid was dried at 120 °C for 12 h, followed by calcination in a N_2 flow (30 ml min^{-1}) at temperatures 550 °C for 1.5 h to obtain the final catalyst, which was designated as Cs/SiO_2. The catalysts with other metal chlorides were prepared in a similar manner, and were designated as K/SiO_2, Na/SiO_2, Zn/SiO_2, Mn/SiO_2 and Ni/SiO_2.

2.2. Catalyst characterizations

Actual contents of metal and chlorine in catalysts were determined by an X-ray fluorescence spectrometry (XRF) on a Shimadzu XRF-1800 spectrometer operated at 70 mA and 40 kV. Surface areas of the catalysts were determined from N_2 adsorption isotherms at 77 K on a Quantachrome Autosorb-1 system through the Brunauer-Emmet-Teller (BET) method. Before the measurement, the samples were degassed under vacuum at 200 °C for 4 h. The pore size distribution was determined from the desorption branches using the Barrett–Joyner–Halenda (BJH) method.

Powder X-ray diffraction (XRD) patterns were recorded on a Bruker D8 ADVANCE powder diffractometer operated at 40 mA and 40 kV equipped with a Cu Kα radiation (λ = 0.15418 nm). The patterns were taken in a 2θ range from 10 to 80 °, with a scanning speed of 0.067 ° s^{-1}.

Fourier transform infrared spectroscopy (FT-IR) spectra were recorded on a NEXUS670 spectrometer in the range of 400-4000 cm^{-1} at room temperature. All obtained spectra were auto-baseline corrected.

The temperature-programmed desorption of CO_2 (CO_2-TPD) measurement was carried out in a quartz microreactor with an inner diameter of 6 mm. Prior to the test, 0.2 g of the catalyst was loaded in the middle of reactor and pretreated in an N_2 flow (30 ml min^{-1}) at 550 °C for 90 min, then saturated with pure CO_2 flow (30 ml min^{-1}) for 20 min after cooling to 50 °C. Weakly adsorbed CO_2 was removed by purging N_2 flow at 80 °C for 40 min. The CO_2-TPD profile was recorded on an Ominstar-200 mass spectrometer (m/e = 44) with a heating rate of 10 °C min^{-1} from 80 to 520 °C in a He flow.

The temperature-programmed desorption of ammonia (NH_3-TPD) measurement was carried out in a quartz microreactor with an inner diameter of 6 mm. Prior to the test, 0.2 g of the catalyst was placed in the middle of reactor and pretreated in air at 550 °C for 90 min, and then cooled to 55 °C under N_2 flow (30 ml min^{-1}). Then, the sample was saturated with 20 ml min^{-1} pure NH_3 flow at 55 °C for 20 min. Weakly adsorbed NH_3 was removed by purging N_2 flow at 100 °C for 40 min. The NH_3-TPD profile was recorded on gas chromatograph with a TCD detector with a heating rate of 10 °C min^{-1} from 100 to 650 °C in an Ar flow.

The properties of acidic sites were determined by in situ Fourier transform infrared (FTIR) spectroscopy of pyridine adsorption, which was performed on a Bruker TENSOR 27 FT-IR spectrometer. The sample was pressed into a 13 mm self-supported wafer and placed into an in situ IR cell. It was then heated from room temperature to 350 °C at a rate of 10 °C min^{-1} under vacuum. The sample was held at 350 °C for 2 h and then cooled to room temperature, and then it was exposed to pyridine vapor for 10 min at room temperature. Then it was purged at 150 °C for 30 min in a He flow, followed by the spectrum recording in the range of 1400 - 1700 cm^{-1} with 32 scans and at a resolution of 4 cm^{-1}.

The Raman spectra of the catalysts were collected on a Renishaw Invia instrument using an excitation laser with wavelength of 325 nm under ambient condition, with a laser power of 3 mW, a dwell time of 60 s, a number of scans of 4 and a resolution of 1 cm^{-1}.

X-ray photoelectron spectroscopy (XPS) was recorded on an ESCALAB 250Xi spectrometer using an Al anode Kα radiation (1486.6 eV). All binding energies were referenced to the Si 2p peak at 103.5 eV of SiO_2 to correct the shift caused by charge effect.

The charge distribution were calculated at B3LYP/6-311 + G(d,p) level [22] by means of the natural bond orbital (NBO) program within the Gaussian 03 package.

2.3. Catalytic reaction

Gas phase dehydrochlorination of TCE was carried out in a quartz tubular fixed-bed reactor (i.d. = 8 mm) at atmospheric pressure. Generally, 0.3 g of the catalyst was loaded in the reactor. A thermalcouple was placed in the middle of the catalyst bed to monitor the actual reaction temperature. Prior to reaction the catalyst was thermally treated at 550 °C for 90 min at a heating rate of 20 °C min^{-1} in N_2 (30 ml min^{-1}), and then was cooled down to the reaction temperature

of 350 °C. The TCE (Aladdin, 99%) and water vapor were introduced to the reactor system by flowing N_2 (10 ml min^{-1}) through a TCE bubbler kept at 0 °C and subsequently a H_2O bubbler kept at 34 °C. Therefore, the concentration of TCE in the feed stream was 6600 ppm and the H_2O was 5 mol. %. The effluent streams were analyzed by an Agilent 6850 gas chromatograph equipped with a flame ionization detector and an Agilent capillary column (DB-1, 30 m x 0.32 mm x 0.26 μm). In addition, reference tests were carried out to control a certain range of TCE conversion (below 30 %) by varying the amount of catalyst. Carbon balances were close to 100 ± 5%. The TCE conversion and product selectivity were defined as follows:

TCE conversion = mol of all detectable products / mol of TCE in feed.

Product selectivity = mol of target product / mol of all detectable products.

It should be noted that the calculated conversion and selectivity may contain certain deviation due to the possible deposition of carbonaceous species on the catalyst surface.

The kinetic study was performed on the same reactor as mentioned above. The feed gases were measured with mass flow controllers and mixed prior to the reactor inlet. For kinetic measurements, the reactor was operated in a differential mode with the TCE conversion less than15%. In typical kinetic tests, 0.1 g catalyst in 100 - 120 mesh was diluted with quartz, and the partial pressure of TCE was adjusted by changing the molar ratio of TCE/N_2 while keeping the total flow rate at 10 ml min^{-1} (by changing the temperature of TCE bubbler the concontration of TCE could be adjusted). Also, the absence of mass transport resistances was checked by Weisz - Prater criterion for internal diffusion and Mears' criterion for external diffusion and the absence of heat transfer was checked by Mears' criterion [23] (See Supplementary Information for detailed calculation). For example, on the Zn/SiO_2 catalyst, the calculated values under kinetic conditions are 1.26×10^{-4} for the Weisz–Prater criterion for internal diffusion, 2.32×10^{-4} for the Mears' criterion for external diffusion, and 0.95×10^{-3} for the Mears' criterion for heat transfer. Those results ensure plug-flow and isothermal conditions within the catalyst bed.

3. Results

3.1. Catalyst characterizations

Fig. 1 shows the N_2 adsorption / desorption isotherm and the pore-size distribution of the catalysts. As shown in Fig. 1a, all the isotherms of the catalysts are similar to the SiO_2 support with a typical H2-type hysteresis loop at a high relative pressure, demonstrating the mesoporous characteristics. All the samples show similar pore sizes (5 −15 nm), which are centered at 10 nm (Fig. 1b).

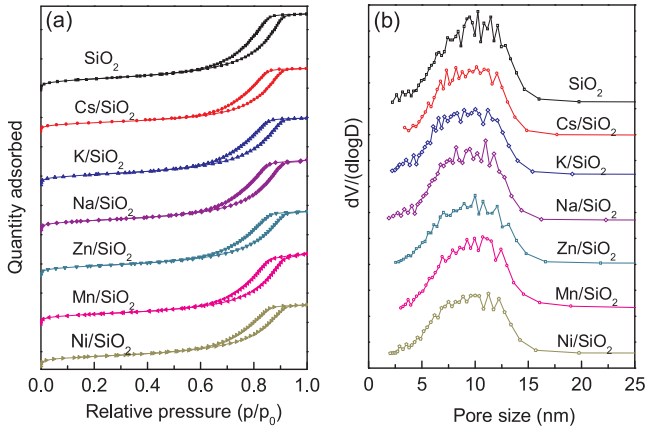

Fig. 1. (a) N_2 adsorption-desorption isotherms and (b) distribution of pore sizes of various catalysts.

Table 1
Physical properties of various catalysts.

Catalyst	S_{BET} (m^2 g^{-1})	Pore size (nm)	Pore volume (cm^3 g^{-1})	Metal Loading (mol%)	Ratio of chlorine/metal (mol/mol)
SiO_2	345	11.6	1.00	-	-
Cs/SiO_2	271	10.3	0.83	5.3	0.97
K/SiO_2	314	10.2	0.88	5.5	1.01
Na/SiO_2	308	10.0	0.93	5.6	1.09
Zn/SiO_2	293	10.5	0.84	4.9	0.88
Mn/SiO_2	296	10.5	0.92	4.8	0.11
Ni/SiO_2	301	10.1	0.81	4.6	0.11

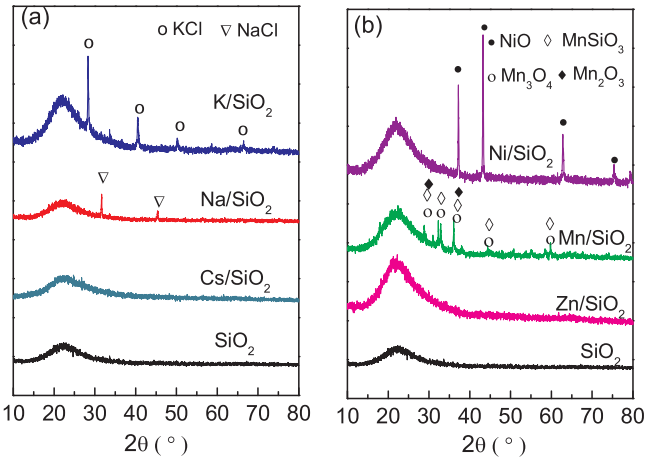

Fig. 2. XRD patterns of various catalysts. (a) Cs/SiO_2, K/SiO_2 and Na/SiO_2; (b) Zn/SiO_2, Ni/SiO_2 and Mn/SiO_2.

Table 1 summarizes the physical properties of the catalysts. The supported catalysts have slightly lower surface areas, smaller average pore sizes and pore volumes compared to those of the SiO_2, due to the blockage of the porous channels of SiO_2 by the impregnation of the metal additives. The actual metal contents in the catalysts are very close to the nominal values, while the contents of chlorine in the catalysts differ very much. For the supported CsCl, KCl and NaCl catalysts, the metal/ chlorine molar ratios are close to 1, indicating there is no loss of chlorine during the calcination process in the catalyst preparation. However, when the $ZnCl_2$, $MnCl_2$ and $NiCl_2$ were used as precursors, the resulting catalysts contain much less chlorine than the nominal value, indicating the decomposition of MCl_2 (M = Zn, Mn, Ni) precursors during the calcination treatment in the catalyst preparation. Especially, for the Mn/SiO_2 and Ni/SiO_2 catalyst, it is found that the chlorine species almost disappear, indicating that the original metal chlorides transform to new species, probably to metal oxides due to the thermal decomposition of metal chlorides. All the metal species in the catalysts are cationic, as revealed by the XPS results (Fig. S1).

Fig. 2 displays the XRD patterns of the catalysts. For the supported alkali metal catalysts (Fig. 2a), characteristic diffractions of KCl (JCPDS No. 99-0101) and NaCl (JCPDS No. 77-2064) are observed in the K/SiO_2 and Na/SiO_2 catalysts, respectively. Since no diffraction of CsCl species could be observed in the Cs/SiO_2 catalyst, it implies the high dispersion of CsCl species on the SiO_2 support. In Fig. 2b, no metal chloride species is detected in the Ni/SiO_2 and Mn/SiO_2 catalysts, instead, metal oxides or silicate are formed in both catalysts, i.e., NiO in the Ni/SiO_2 (JCPDS No. 04-0850), Mn_3O_4 (JCPDS No. 24-0374), Mn_2O_3(JCPDS No. 06-0540) and $MnSiO_3$ (JCPDS No. 12-0181) in the Mn/SiO_2. No apparent diffraction of zinc species could be found in the Zn/SiO_2 catalyst, indicating that the high dispersion of Zn species on the SiO_2 support.

The surface features of the catalysts were investigated by FTIR and the results are shown in Fig. 3. All the catalysts show three distinct

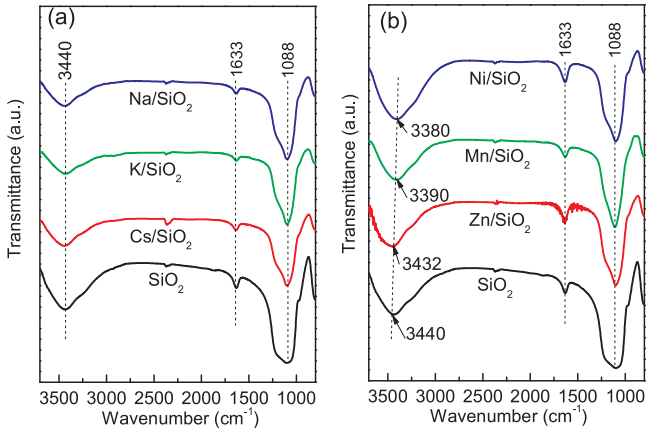

Fig. 3. FTIR spectra of (a) Cs/SiO_2, K/SiO_2 and Na/SiO_2; and (b) Zn/SiO_2, Ni/SiO_2 and Mn/SiO_2 catalysts.

bands. The band at about 3440 cm^{-1} is attributed to the surface Si-OH group, the weak band at 1633 cm^{-1} is assigned to the bending vibration of the hydroxyl group, and the broadband at 1088 cm^{-1} is assigned to asymmetric vibration of Si-O-Si in the SiO_2 support [24]. As can be seen in Fig. 3a, the relative intensity of the Si-OH band at 3440 cm^{-1} show some decreases in alkali metal (Cs, K, Na) catalysts when comparing with the SiO_2 support, suggesting that a portion of the surface Si-OH groups had been consumed via alkali metal chlorides [25–27]. The supported transition metal catalysts show significant red-shift for the Si-OH band at 3340 cm^{-1} (Fig. 3b) compared to that of the SiO_2, implying that new species formed with an interaction between the transition metal and the support SiO_2 surface [28]. For example, zinc specie of –O–Zn–Cl in Zn/SiO_2 [29,30], metal silicate species in Mn/SiO_2 and Ni/SiO_2 [31]. The formation of manganese silicate species could be found in the XRD results (Fig. 2b). However, no apparent diffraction of nickel silicate species could be detected in the XRD patterns, which most probably due to the formation of amorphous or highly dispersed nickel silicate species [32].

Fig. 4 shows the CO_2-TPD and NH_3-TPD profiles of the catalysts to determine their surface basicity and acidity, respectively. Similar to the SiO_2 support, the supported transition metal catalysts have weak CO_2 desorption peaks at low temperature (about 100 °C), probably due to the impurities in the catalysts or the desorption of physisorbed CO_2. The Na/SiO_2 catalyst shows no distinct surface basicity, while the K/SiO_2 and Cs/SiO_2 catalysts show obvious CO_2 desorption peaks at about 200 °C, which could be assigned to the moderate basic sites [33–35]. In addition, the Cs/SiO_2 has much larger peak area and slightly higher

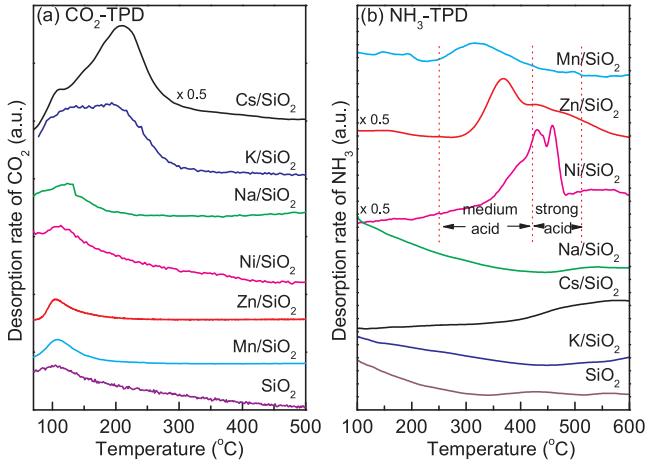

Fig. 4. (a) CO_2-TPD and (b) NH_3-TPD profiles of various catalysts.

desorption temperature than the K/SiO_2, suggesting the former has higher amount of surface basic sites and higher basicity strength. A decreasing order in the basicity strength of catalysts follows: Cs/SiO_2 > K/SiO_2 > Na/SiO_2. This trend is also confirmed by the O1s XPS spectra of these catalysts (Fig S2). The O1s binding energy at 532.9 eV assigning to surface oxygen species (e.g. adsorbed oxygen and surface hydroxyl groups) shifts to a lower value (532.6 eV) in supported alkali metal catalysts, which indicated gradually increasing basicity [36,37]. The enhanced basicity strength in alkali metal catalyst is due to the Si–O–M (M = Cs, K) species formed on the catalyst surface reinforced the basic strength of the O^{2-} in the Si–O–M structure [27]. The NH_3-TPD profiles of the catalysts (Fig. 4b) reveal that the supported alkali metal catalysts show no NH_3-desorption peaks below 500 °C, while the supported transition metal catalysts have obvious intense NH_3-desorption peaks in the range of 300 - 500 °C, indicating the existence of the medium and strong acid sites on supported transition metal catalysts [38–41]. Specifically, the Zn/SiO_2 and Mn/SiO_2 catalysts contain mainly the medium acidic sites (in NH_3 desorption range of 250-400 °C), while the Ni/SiO_2 contains both medium and strong acidic sites (in NH_3 desorption range of 400-500 °C). Besides, it seems that the acid strength of these catalysts follows the order of Mn/SiO_2 < Zn/SiO_2 < Ni/SiO_2, as the NH_3-desoprtion peaks of these catalysts generally shift to higher temperature.

The nature of the surface acidity of the supported transition metal catalysts were further determined by FTIR spectra of pyridine adsorption and the results are shown in Fig. 5. All the catalysts show three bands at about 1600, 1490 and 1450 cm^{-1}. The bands at 1600 and 1450 cm^{-1} are assigned to the surface Lewis acid sites and the band at 1490 cm^{-1} is assigned to the combination of Lewis and Brönsted acid sites [42–45]. Particularly, the Ni/SiO_2 shows two overlapped bands at 1600 and 1612 cm^{-1}, which could be assigned to the weak and strong Lewis acid sites, respectively [46,47].

The presence of surface acid sites on the SiO_2-supported transition metal catalysts has been well documented in literature and it has been recognized that the acid sites on silica-supported oxides (such as ZnO, NiO) are usually considered as the Lewis acid centers [48–51]. As for the Brönsted acid sites, Upadhyaya et al. [30]

reported a silica supported zinc catalyst using $ZnCl_2$ as the precursor containing dominant Lewis acid sites and minor Brönsted acid sites due

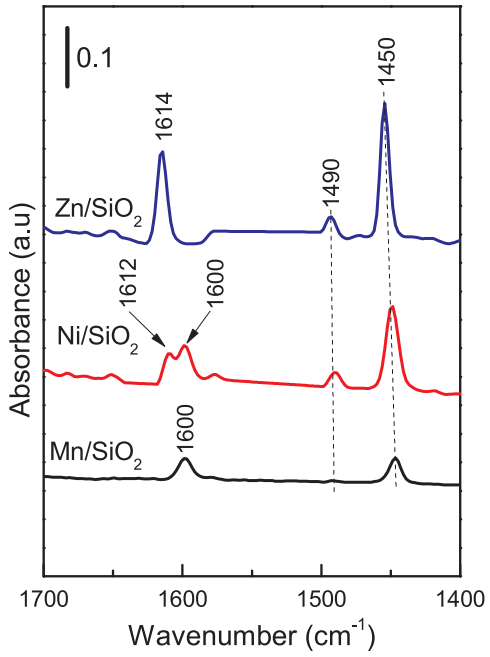

Fig. 5. FTIR spectra of pyridine adsorption on Zn/SiO_2, Mn/SiO_2 and Ni/SiO_2 catalysts.

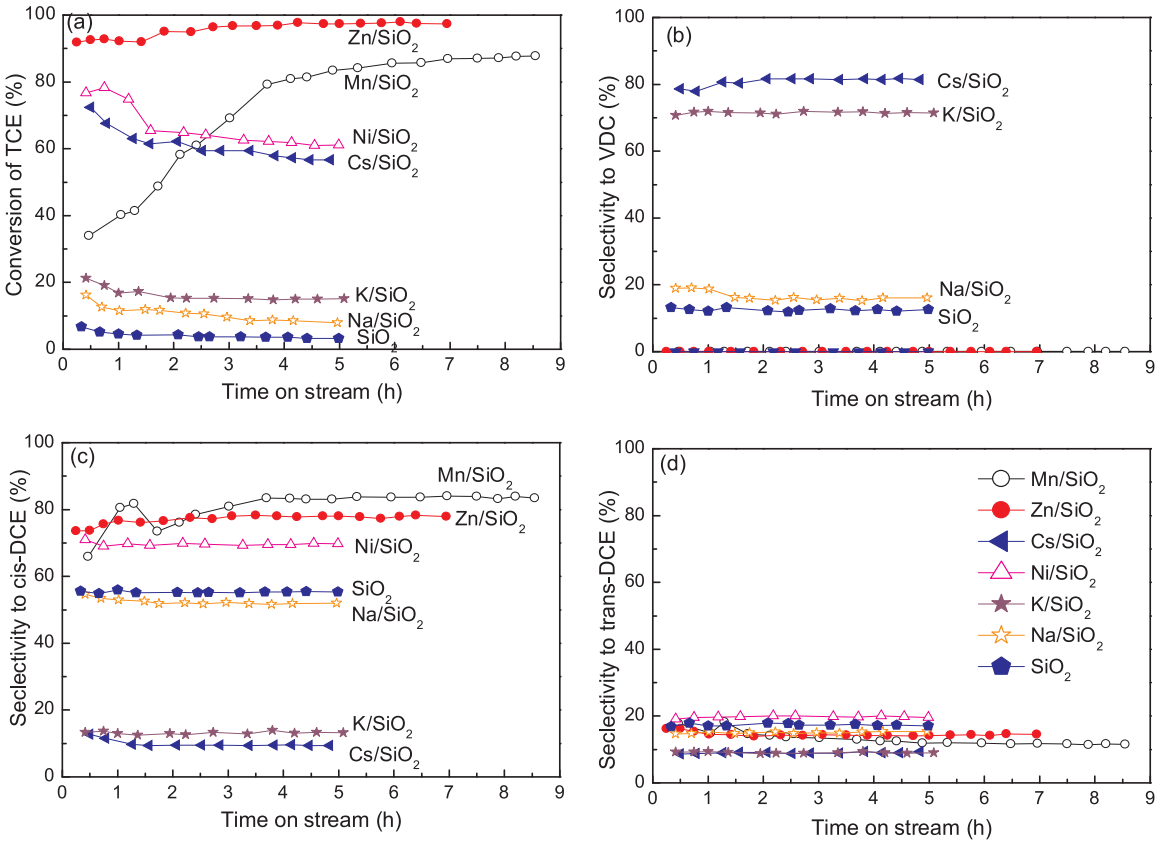

Fig. 6. (a) conversion of TCE; (b) selectivity to vinylidene chloride (VDC); (c) selectivity to cis-1, 2-dichloroethene (cis-DCE) and (d) selectivity to trans-1, 2-dichloroethene (trans-DCE) over various catalysts.
catalyst loading = 0.3 g; pretreatment temperature = 550 °C; reaction temperature = 350 °C; H_2O content = 5 mol.%.

to the formation of -O-Zn-Cl [29]. Moreover, it was reported that nickel silicate possessed acidity [52–55]. There are both Brönsted acid sites and Lewis acid sites on the surface of the nickel silicate, especially the latter when the nickel silicate is pretreated above 400 °C [55]. Lehmann et al. [56] also suggested both Lewis acid sites and Brönsted acid sites coexisted in a sample of MCM-41 supported nickel due to nickel oxide and nickel silicate. It was also reported that all acid sites in silica supported manganese oxide catalyst almost could be assigned to Lewis acid sites [57]. Therefore, the current results (Fig. 5) are in perfect agreement with those in literature, namely, the Zn/SiO_2 and Ni/SiO_2 catalysts contain dominant Lewis acid sites and limited Brönsted acid sites, while the Mn/SiO_2 only contains Lewis acid sites as the band at 1490 cm^{-1} is absent in this catalyst.

3.2. Catalytic testing

Fig. 6 shows the catalytic performance of the catalysts and the detailed results are also summarized in Table 2. As can be seen in Fig. 6a, all the catalysts give relatively stable TCE conversion (quasi-steady) at 350 °C after 3 h reaction. The SiO_2 support shows low TCE conversion (3.6 %), the Na/SiO_2 gives higher TCE conversion (10 %) compared to that of the SiO_2, while the K/SiO_2 gives about 15 % of TCE conversion. Interestingly, the Cs/SiO_2 catalyst shows much higher TCE conversion (69.3 %). The Zn/SiO_2 and Mn/SiO_2 catalysts give very high TCE conversions (about 90%), while the TCE conversion on the Ni/SiO_2 is slightly lower (61.8 %). The supported transition metal catalysts are generally more active than the supported alkali metal catalysts. Particularly, it is found that the TCE conversions on the Zn/SiO_2 and Mn/SiO_2 slightly increase with reaction time (for the Zn/SiO_2 catalyst the conversion increases from 91.9 % to 97.4 % after 5 h reaction and for the Mn/SiO_2 catalyst the conversion increases from 84.7 % to 87.7 % after 5 h reaction). These catalysts are generally stable under the reaction conditions, except that the Cs/SiO_2 and Ni/SiO_2 slightly deactivate in the first 2 h reaction. Concerning the product selectivity, the main products are VDC and 1,2-DCE (including cis-DCE and trans-DCE), and the minor products are vinyl chloride ($HCl_2CCH_2Cl \rightarrow HClC = CH_2 + Cl_2$) and trichloroethylene ($HCl_2CCH_2Cl \rightarrow Cl_2C = CHCl + H_2$). The supported alkali metal catalysts (Cs/SiO_2 and K/SiO_2) show a high selectivity to VDC (71-81%) and a low selectivity to 1,2-DCE (18 - 22 %, equals to (selectivity to cis-DCE + selectivity to trans-DCE)); while the

Table 2
Catalytic performance of various catalysts for dehydrochlorination of TCE.

Catalyst	Conv.[a] (%)	Selectivity (%)					
		VDC	cis-DCE	trans-DCE	vinyl chloride	trichloroethylene	cis-/trans-DCE ratio
SiO_2	3.6	12.5	55.4	17.0	10.9	4.2	3.2
Na/SiO_2	10.0	16.0	51.8	15.4	11.8	5.0	3.3
K/SiO_2	15.1	71.5	13.2	9.0	6.3	0	1.4
Cs/SiO_2	69.3	81.5	9.3	8.9	0.2	0.1	1.0
Zn/SiO_2	97.4	0.0	77.9	14.3	7.8	0	5.4
Mn/SiO_2	86.0	0.0	83.7	11.6	4.7	0	7.2
Ni/SiO_2	61.8	0.0	69.8	20.0	9.6	0.6	3.4

[a] All data were taken after 5 h reaction; Reaction temperature = 350 °C, catalyst loading = 0.3 g, H_2O content = 5 mol. %.

SiO_2 and Na/SiO_2 show a low selectivity to VDC (12- 17%) and a high selectivity to 1,2-DCE (67 - 72 %). For the supported transition metal catalysts (Mn/SiO_2, Ni/SiO_2 and Zn/SiO_2), they give almost no selectivity to VDC and very high selectivity to 1,2-DCE (up to 95 %). Moreover, it is found (Fig. 6c–d) that these catalysts give high a selectivity to cis-DCE (69-84%) and a low selectivity to trans-DCE (about 15%). One thing must be concerned is the possible hydrolysis of Cl-containing hydrocarbons in the presence of H_2O under reaction conditions. Under our analysis conditions, no other Cl-containing hydrocarbons than the mentioned products were detected, indicating that such hydrolysis reaction is negligible under the reaction conditions. Indeed, it was reported that the reaction between H_2O and chlorinated hydrocarbons usually needs high reaction temperature (e.g. 400 °C). For example, Feijen-Jeurissen et al. [58] reported that 1,1,2-trichloroethylene would not react with H_2O over γ-Al_2O_3 until the reaction temperature was higher than 350 °C.

Also, we compared the catalytic performance of the catalysts under dry reaction conditions (in the absence of H_2O) and the results are shown in Table S1 and Fig. S3. The comparison of the results under dry and wet conditions suggests that: 1, the presence of H_2O in the feed stream suppresses the catalytic activity to some extent both in the initial and quasi-steady stages, probably due to the blockage of active sites by competitive adsorption of H_2O on the catalyst surface; 2, the presence of H_2O hardly changes the product selectivity; 3, the presence of H_2O improves the catalyst stability. For example, the Ni/SiO_2 catalyst deactivates rapidly in the absence of H_2O, with a TCE conversion of 40.0 % after 2 h; while in the presence of H_2O the deactivation is much alleviated, with a TCE conversion of 61.8 % after 2 h reaction.

It is well known that the product selectivity is also related to the reactant conversion. To clarify this point, we have tried to control the TCE conversion at similar levels by changing the catalyst loading while keeping other parameters (reaction temperature and space velocity) constant. Comparing the results summarized in Tables S3 and 2, it is found that the product selectivities (VDC, cis-DCE and trans-DCE) do not change at either high or low TCE conversion, which suggests the product selectivity is dependent on the nature of the catalyst rather than on thermodynamics.

3.3. Kinetic investigation

Kinetic investigations were conducted on Cs/SiO_2, Na/SiO_2 and Zn/SiO_2 catalysts, representing basic, neutral and acidic catalysts, respectively. As shown in Table 3 and Fig. 7 (see Tables S3 and S4 for detailed data), the power law rate expressions of the catalysts are: $r = 5.53 \times 10^{-8} [P_{TCE}]^{0.85 \pm 0.03}$ for the Cs/SiO_2 catalyst; $r = 0.68 \times 10^{-8} [P_{TCE}]^{0.94 \pm 0.02}$ for the Na/SiO_2 catalyst; $r = 32.82 \times 10^{-8} [P_{TCE}]^{0.65 \pm 0.05}$ for the Zn/SiO_2 catalyst. The parity plots and residual analyses (Fig. S4) indicate that the deduced rate expressions are valid. In addition, the calculated activation energies (Ea) show that the Ea for the Zn/SiO_2 is 92.2 ± 2.1 kJ mol^{-1}, which is significantly lower than those for the Cs/SiO_2 and Na/SiO_2 catalysts (118.1 ± 0.4 and 142.4 ± 3.7 kJ mol^{-1}, respectively). The calculated pre-exponential factor increases from the most active Zn/SiO_2 (60.4) to the least active Na/SiO_2 (4.03×10^4), indicating a typical compensation effect.

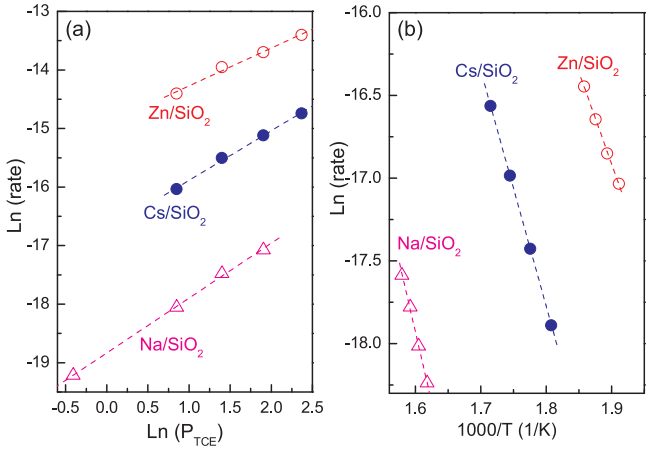

Fig. 7. (a) Dependence of reaction rates on TCE partial pressures and (b) Arrhenius plots of various catalysts.

4. Discussion

4.1. Catalytic activity, catalyst deactivation and the role of H_2O

It is found that the catalysts employed in the current work show very different activities, namely, the supported transition metal catalysts are generally more active than the supported alkali metal catalysts (Table 2 and Fig. 6a). Furthermore, the intrinsic activities (turnover frequencies, TOFs) are evaluated according to the kinetic results. Under certain reaction conditions (TCE partial pressure = 2.341 kPa, reaction temperature = 310 °C), TOFs based on the mass reaction rate (mol g^{-1} s^{-1}, data taken from Table S3) divided by the moles of metal atom in the catalyst (data taken from Table 1) are calculated to be 7.4×10^{-4} s^{-1} for the Zn/SiO_2, 1.5×10^{-4} s^{-1} for the Cs/SiO_2, and 0.18×10^{-4} s^{-1} for the Na/SiO_2. The TOF of the Zn/SiO_2 is 5 times as high as that of the Cs/SiO_2 and 40 times as high as that of the Na/SiO_2, which could be explained based on the kinetic results. On one hand, it is found that the Zn/SiO_2 catalyst has the highest rate constant (32.82×10^{-8}), which suggests that the transition metal Zn is intrinsically more active than the alkali metals Cs and Na. On the other hand, it is found that the reaction orders of TCE for the Zn/SiO_2, Cs/SiO_2 and Na/SiO_2 catalyst are 0.65, 0.85 and 0.94, respectively (Note that due to the insufficient data points, these values may contain certain errors). Assuming that the dehydrochlorination of TCE on the catalyst obeys a classic Langmuir-Hinshelwood (L-H) mechanism which involves adsorption and activation of TCE molecules on the surface sites, then the lowest reaction order of TCE on the Zn/SiO_2 suggests the highest surface coverage of reactant molecules on this catalyst. This is probably due to the presence of acid sites in the Zn/SiO_2, which provides adsorption centers for TCE molecules [59–61] and thus explains its highest TOF. However, it should be noticed that on the base Cs/SiO_2 catalyst, the TCE reaction order of 0.85 implies possible adsorption of the TCE molecules on the basic sites of the catalyst although such adsorption might be weak, which infers a different reaction mechanism other than that on the acid catalyst and will be discussed in the following section.

Table 3
Summary of kinetic parameters of various catalysts[a].

Catalyst	$r = k P_{TCE}^n$		Activation energy / kJ mol^{-1}	Pre-exponential factor (A)
	k	n		
Cs/SiO_2	5.53×10^{-8}	0.85 ± 0.03	118.1 ± 0.4	1.82×10^3
Na/SiO_2	0.68×10^{-8}	0.94 ± 0.02	142.4 ± 3.7	4.03×10^4
Zn/SiO_2	32.82×10^{-8}	0.65 ± 0.05	92.2 ± 2.1	60.4

[a] reaction temperature = 310 °C, H_2O content = 5 mol.%.

Deactivation has been observed on most of the catalysts, particularly under dry conditions (Fig. S3), while the addition of H_2O improves the catalyst stability (Fig. 6). To illustrate the origin of catalyst deactivation, we analyzed the Raman spectra of the representative Ni/SiO_2 catalyst before and after reaction because its stability is much improved by the H_2O addition. As shown in Fig. S5a, the fresh Ni/SiO_2 catalyst shows no Raman bands while the spent sample in the absence of H_2O shows two distinct Raman bands at 1402 and 1620 cm^{-1} which are assigned to the coke species [62]. Similar scenarios are also observed on the Zn/SiO_2 and Mn/SiO_2 catalysts (Fig. S5b–c). Therefore, it seems that the catalyst deactivation is due to the carbon deposit on the catalyst surface. It is well-known that the catalytic dehydrohalogenation usually involves the interaction between the reactant halogen atoms (e.g. Cl or F) with the acid site of the catalyst [59,60]. The NH_3-TPD results (Fig. 4b) show that the presence of strong acid sites in the Ni/SiO_2 may lead to strong interaction between the TCE and/or product molecules and the catalyst surface, which may account for the observed deactivation due to the blockage of the active sites. Interestingly, when 5 mol.% of water vapor was added in the feed stream, the Raman spectrum of the spent catalyst shows much more less intense bands at 1402 and 1620 cm^{-1}, implying that the addition of H_2O could efficiently remove the surface carbon species and thus maintain the activity. Indeed, the element compositions of the spent catalysts measured by XRF (Table S5) show that the spent catalysts (either under dry or wet condition) have almost identical contents of metal species but slightly higher chlorine/metal molar ratio compared to those of the corresponding fresh ones, which implies the deposition of Cl-containing carbon species on the catalyst surface during the reaction process.

However, the role of H_2O can not be simply attributed to the removal of surface deposits because the introduction of H_2O may also alter the catalyst properties and thus affect the catalytic behaviors. For example, the role of H_2O in dehydrochlorination of TCE was investigated in an early work by Mochida et al. [63] over an alumina catalyst. The authors found that the addition of H_2O in the reaction system enhanced the activity to some extent but significantly changes the product distribution (i.e. the selectivity to VDC changed from 37.1 % in the absence of H_2O to 81.4 % in the presence of H_2O, while the selecivity to 1,2 -DCE changed from 62.7% in the absence of H_2O to 18.6 % in the presence of H_2O). Such drastic changes in the catalytic behaviors particularly the selectivity was explained by the decrease in the surface acidity induced by the hydration of the Al_2O_3. Catalyst hydration via the reaction between H_2O and metal oxide was also evidenced over basic oxides (such as lanthanide oxide and alkaline earth oxides) for catalytic destruction of chlorinated hydrocarbons (e.g. CCl_4, $CHCl_3$ and CH_2Cl_2) by Van der Avert and Weckhuysen [64,65]. The authors concluded that the lanthanum hydroxide was formed in the presence of steam at the reaction temperature (250-350 °C) then was partially transformed to a chlorinated lanthanide oxide (which was regarded as the active sites) during the catalytic reaction. Moreover, in our recent work on catalytic dehydrochlorination of TCE to VDC over SiO_2-supported Mg catalysts, active Mg(OH)Cl surface species could be formed using $Mg(NO_3)_2{\cdot}6H_2O$ and $MgCl_2{\cdot}6H_2O$ as the precursors [10]. Therefore, the H_2O-induced generation of new surface species (e.g. hydrated or partially hydrated metal species) on the catalysts could not be ruled out. One hint of such speculation is that the TCE conversions on the Zn/SiO_2 and Mn/SiO_2 slightly increase with reaction time (Fig. 6a). However, detailed characterizations such as in-situ spectroscopic study are required in order to reach a concrete conclusion.

4.2. The roles of surface basicity and acidity on the product selectivity

In addition to the different activities, the product selectivities differ very much on these catalysts, namely, the basic alkali metal catalysts (e.g. K/SiO_2 and Cs/SiO_2) tend to produce VDC, the neutral catalysts (e.g. SiO_2 and Na/SiO_2) and acidic transition metal catalysts (e.g. Zn/SiO_2, Mn/SiO_2 and Ni/SiO_2) tend to produce 1, 2-DCE. This observation is in good agreement with the previous reports [11]. However, it is worthwhile to put more detailed discussion on the roles of surface basicity and acidity on the product distributions, particularly in respect of the strength of basicitiy and acidity.

First of all, in the current work, the CO_2-TPD (Fig. 4a) and O1s XPS (Fig. S2) results reveal that the basicity strength of the supported alkali metal catalysts follows the order of $K/SiO_2 < Cs/SiO_2$. Meanwhile, the VDC selectivities for these two catalysts increase in the order of K/SiO_2 (72%) < Cs/SiO_2 (82%). The correlation between the surface basicity and VDC selectivity leads to a conclusion that stronger base is more favorable for the formation of VDC. This conclusion is also supported by the previous findings that very strong basic compounds such as organic amine [20] and NaOH [66] gave extremely high VDC selectivity (up to 99 %).

Secondly, the neutral catalysts such as SiO_2 and Na/SiO_2 also show higher 1, 2-DCE selectivity (65-75%) than VDC selectivity (10-20%), Thus it is reasonable to conclude that the neutral catalysts are more favorable to the formation of 1, 2-DCE.

Thirdly, it is apparent that the acid strength of the catalyst exerts an important impact on the distributions of the cis-DCE and trans-DCE, namely, the ratio of cis-DCE/trans-DCE. As shown in Table 2, the cis-DCE/trans-DCE ratios are 3.4, 5.4 and 7.2 for the Ni/SiO_2, Zn/SiO_2 and Mn/SiO_2, respectively. Such ascending trend is consistent with the increasing acid strength of these catalysts, as the NH_3-TPD results (Fig. 4b) clear show that the acid strength follows an order of $Mn/SiO_2 < Zn/SiO_2 < Ni/SiO_2$. It implies that the medium acid sites tend to produce cis-DCE while the strong acid sites tend to produce trans-DCE. Moreover, it seems that the acid type (e.g. Lewis acid or Brönsted acid) may also affect the product distribution. The FTIR spectra of pyridine adsorption (Fig. 5) suggests that the Zn/SiO_2 and Ni/SiO_2 contain majority of Lewis acid sites and minority of Brönsted acid sites, while the Mn/SiO_2 contains only Lewis acid sites. As the highest selectivity to cis-DCE is obtained on the Mn/SiO_2 (83.7%, Table 2), it implies that Lewis acid sites are favorable for the formation of cis-DCE but Brönsted acid are favorable for the formation of trans-DCE. Although the nature of the role of Lewis/Brönsted acid sites on the product distribution remains unclear at present, such implication is supported by our recent findings on the dehydrochlorination of TCE over Cr_2O_3 catalysts. It was found that very high selectivity to cis-DCE (up to 91%, Fig. S6) was obtained on the Cr_2O_3 with exclusively surface Lewis acid sites [67–71].

4.3. Possible mechanisms of TCE dehydrochlorination on different catalysts

The current results clearly show the very different behaviors of the catalysts, which implies various reaction pathways on these catalysts. Therefore, the possible reaction mechanisms on these catalysts are proposed.

We first analyzed the charge distributions of the TCE molecule by DFT calculation (Fig. S7). It can be seen that the charge densities of the Cl atoms attached to the α-C are -0.088 eV, while that of the H atom attached to the α-C is 0.251 eV. In contrast, the charge density of the Cl atom connected to the β-C is 0.041 eV, while those of the H atoms connected to the β-C are 0.219 eV. The results imply that the the Cl atom on the α-C could interact with the acid site (electron acceptor) while the H atom on the α-C could interact with the base site (electron donor).

Based on the charge distribution analysis and the observed catalytic behaviors, different reaction mechanisms on the basic, neutral and acidic catalysts could be proposed, as shown in Fig. 8. For the basic catalysts (e.g. K/SiO_2 and Cs/SiO_2), an E1cb mechanism is proposed. In the molecular structure of TCE, the H atom attached to the α-C would react with the base site on the catalyst. After its extraction a carbanion intermediate is formed. Subsequently, the departure of the Cl atom attached to the β-C atom leads to the formation of VDC.

For the neutral catalysts (e.g. SiO_2 and Na/SiO_2), an E2 concerted

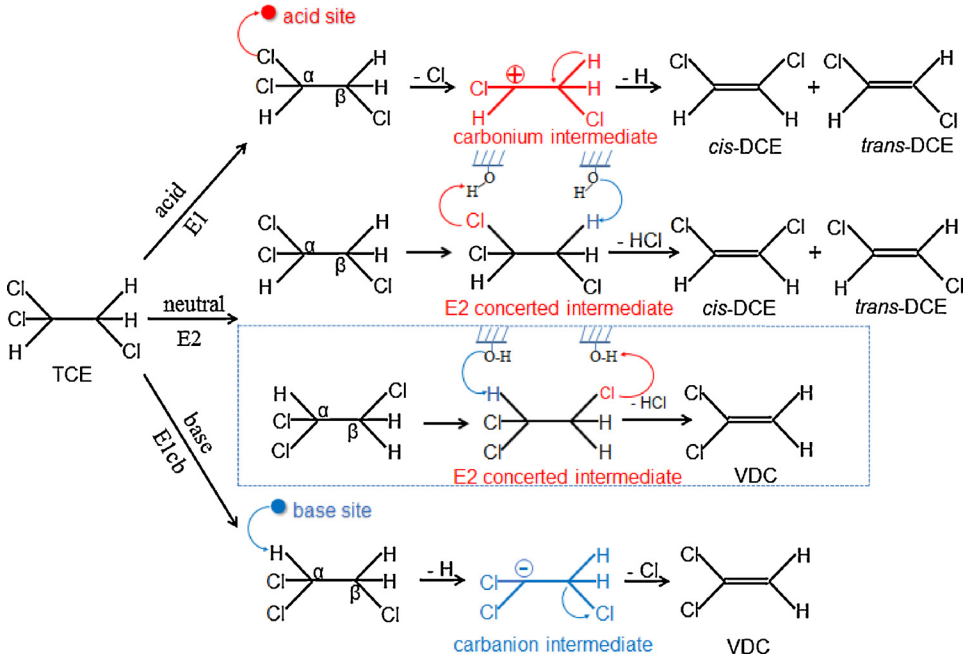

Fig. 8. possible reaction mechanisms on different catalysts.

mechanism (bimolecular elimination) mechanism is proposed. It is well-known that SiO_2 contains abundant surface hydroxyl (-OH) groups, which can act either acid sites or base sites [72,73]. In such case, the acid site will interact with the Cl atom on the α-C while the base site will interact with the H atom on the β-C, and thus leads to the formation of cis-DCE and trans-DCE. However, it is also possible that the interaction between acid site and Cl atom on the β-C, and that between base site and H atom on the α-C leads to the formation of VDC. Judging from the selectivities obtained on the neutral catalysts, it seems that the former reaction (Cl on α-C reacts with acid site and H on β-C reacts with base site) more likely occurs than the latter one (Cl on β-C reacts with

acid site and H atom on α-C reacts with base site).

For the acid catalysts (e.g. Ni/SiO_2, Zn/SiO_2 and Mn/SiO_2), an E1 mechanism is proposed. The Cl atom on the α-C would be extracted by its interaction with the acid site of the catalyst, leading to the formation of a carbonium intermediate. Subsequently, the departure of H atom on the β-C, leads to the formation of cis-DCE and trans-DCE.

It should be noticed that the proposed reaction mechanisms are quite simplified and actual reaction taking place on the catalyst may contains mixed routes, which results in the presence of various products. For example, the selectivity to 1,2-DCE (about 20 %) on the K/SiO_2 and Cs/SiO_2 may result from individual contributions from the base metals (K and Cs) and the neutral SiO_2 but it also seems that the contribution from the base metal is more pronounced than that from the SiO_2 support. Nonetheless, a general picture could be established based on the above results and discussion. As shown in Fig. 9, on the base catalysts, the reaction mainly follows an E1cb mechanism which leads to the formation of VDC; on the neutral catalysts, the reaction may follow an E2 mechanism which leads to the formation of major 1, 2-DCE and minor VDC; on the acid catalysts, the reaction mainly follows an E1 mechanism which leads to almost exclusively 1, 2-DCE.

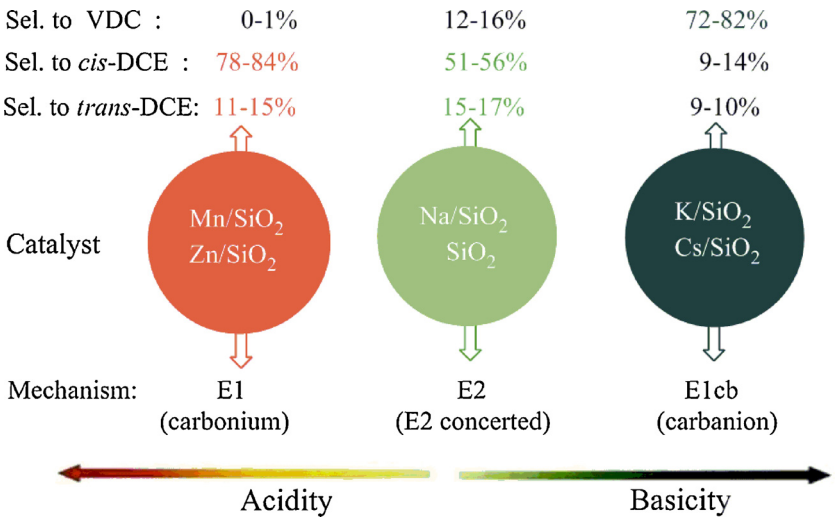

Fig. 9. Influence of the acid-base properties of catalysts on the product selectivity and reaction mechanism.

5. Conclusions

This work demonstrates the important roles of surface acidity and basicity on the tuning of the product distribution in gas-phase dehydrochlorination of TCE. The characterization results show that interaction between metal and SiO_2 support leads to the alternation of surface acidity and basicity. The following conclusions can be obtained: (i) The basicity of catalyst is a key factor for the generation of VDC and stronger base leads to higher VDC selectivity. (ii) The surface medium Lewis acid sites are advantageous for the generation of cis-DCE. (iii) The dehydrochlorination of TCE may proceed through the E1cb mechanism on the base catalysts, the E2 mechanism on the neutral catalysts, and the E1mechanism on acid catalysts.

Acknowledgements

This work is financially supported by the Natural Science Foundation of Zhejiang Province (No. LY14B020001), National Natural Science Foundation of China (Nos. 21643007 and 21773212).

Appendix A. Supplementary data

Supplementary material related to this article can be found, in the online version, at doi:https://doi.org/10.1016/j.apcatb.2018.04.018.

References

[1] I. In, J.T. Houghton, G.J. Jenkins, J.J. Ephraums (Eds.), Climate Change, The IPCC scientific assessment. Report prepared for IPCC by working group I, Cambridge University Press, Cambridge, UK, 1990.
[2] U.N.E.P.O. Secretariat, Handbook for the Montreal protocol on substances that deplete the ozone layer, UNEP/Earthprint, 2006.
[3] J. Stach, V. Pekarek, R. Endrst, J. Hetflejs, Chemosphere 39 (1999) 2391–2399.
[4] A.W.A.M. van der Heijden, A.J.M. Mens, R. Bogerd, B.M. Weckhuysen, Catal. Lett. 122 (2008) 238–246.
[5] J.E. Kester, Encyclopedia of Toxicology, Vinylidene Chloride (VDC) A2 - Wexler, Philip, Third Edition, Academic Press, Oxford, 2014, pp. 942–947.
[6] N.C. Craig, L.G. Piper, V.L. Wheeler, J. Phys. Chem. 75 (1971) 1453–1460.
[7] K. Kokubo, K. Kitasaka, T. Oshima, Org. Lett. 8 (2006) 1597–1600.
[8] D.A. Turton, D.F. Martin, K. Wynne, Phys. Chem. Chem. Phys. 12 (2010) 4191–4200.
[9] M. Chaliha, A. Cusack, M. Currie, Y. Sultanbawa, H. Smyth, J. Agric. Food Chem. 61 (2013) 5738–5745.
[10] C. Tang, Y.X. Jin, J.Q. Lu, X.N. Li, G.Q. Xie, M.F. Luo, Appl. Catal. A 508 (2015) 10–15.
[11] I. Mochida, J. Take, Y. Saito, Y. Yoneda, J. Org. Chem. 32 (1967) 3894–3898.
[12] I. Mochida, Y. Yoneda, The Journal of Organic Chemistry 33 (1968) 2161–2163.
[13] I. Mochida, Y. Anju, H. Yamamoto, A. Kato, T. Seiyama, Bull. Chem. Soc. Jpn. 44 (1971) 3305–3310.
[14] I. Mochida, A. Uchino, H. Fujitsu, K. Takeshita, Chem. Lett. (1975) 745–746.
[15] I. Mochida, T. Miyazaki, T. Takagi, H. Fujitsu, Chem. Lett. (1985) 833–836.
[16] I. Mochida, T. Takagi, H. Fujitsu, Appl. Catal. 18 (1985) 105–115.
[17] H. Fujitsu, T. Takagi, I. Mochida, Bull. Chem. Soc. Jpn. 58 (1985) 1589–1590.
[18] I. Mochida, Y. Yasumoto, H. Fujitsu, Y. Kojima, Chem. Lett. (1992) 461–464.
[19] C. Tian, C.S. Lu, B. Wang, X.Z. Xie, Y.S. Miao, X.N. Li, RSC Adv. 5 (2015) 103829–103833.
[20] C. Tang, Y.X. Jin, X.X. Wang, G.S. Hu, G.Q. Xie, X.N. Li, M.F. Luo, Chem. Res. Chin. Univ. 31 (2015) 787–791.
[21] Y.H. Hu, T.Y. Song, Y.J. Wang, G.S. Hu, G.Q. Xie, M.F. Luo, Acta Physico-Chimica Sinica 33 (2017) 1017–1026.
[22] A.D. Becke, J. Chem. Phys. 98 (1993) 5648–5652.
[23] X. Xie, Y. Li, Z.Q. Liu, M. Haruta, W. Shen, Nature 458 (2009) 746.
[24] Y.Y. Pei, M. Wang, D. Tian, X.F. Xu, L.J. Yuan, J. Colloid Interface Sci. 453 (2015) 194–201.
[25] Y.M. Wang, Z.Y. Wu, J.H. Zhu, J. Solid State Chem. 177 (2004) 3815–3823.
[26] Y.M. Wang, Z.Y. Wu, Y.L. Wei, J.H. Zhu, Microporous Mesoporous Mater. 84 (2005) 127–136.
[27] J.B. Yan, C.L. Zhang, C.L. Ning, Y. Tang, Y. Zhang, L.L. Chen, S. Gao, Z.L. Wang, W.X. Zhang, J. Ind. Eng. Chem. (Amsterdam, Neth.) 25 (2015) 344–351.
[28] Y.S. Liu, G.Z. Wu, H.Y. Fu, Z. Jiang, S.M. Chen, M.L. Sha, Dalton Trans. 39 (2010) 3190–3194.
[29] V.R. Choudhary, K. Mantri, Catal. Lett. 81 (2002) 163–168.
[30] D.J. Upadhyaya, S.D. Samant, Appl. Catal. A 340 (2008) 42–51.
[31] L.F. Zhang, J.F. Lin, Y. Chen, J. Chem. Soc. Faraday Trans. 88 (1992) 2075–2078.
[32] S.R. Kirumakki, B.G. Shpeizer, G.V. Sagar, K.V.R. Chary, A. Clearfield, J. Catal. 242 (2006) 319–331.
[33] Y.J. He, B.L. Yang, G.X. Cheng, Catal. Today 98 (2004) 595–600.
[34] M.H. Wang, H. Wang, N. Zhao, W. Wei, Y.H Sun, Catal. Commun. 7 (2006) 6–10.
[35] J. Gao, J. Guo, D. Liang, Z. Hou, J. Fei, X. Zheng, Int. J. Hydrogen Energy 33 (2008) 5493–5500.
[36] Q.C Li, S.E. Brown, L.J. Broadbelt, J.-G. Zheng, N.Q. Wu, Microporous Mesoporous Mater. 59 (2003) 105–111.
[37] A.C. Oliveira, L. Martins, D. Cardoso, Microporous Mesoporous Mater. 120 (2009) 206–213.
[38] P. Berteau, B. Delmon, Catal. Today 5 (1989) 121–137.
[39] M. Lewandowski, Z. Sarbak, Fuel 79 (2000) 487–495.
[40] C. García-Sancho, I. Agirrezabal-Telleria, M. Güemez, P. Maireles-Torres, Appl. Catal., B 152 (2014) 1–10.
[41] A. Ciftci, D.M. Ligthart, A.O. Sen, A.J. van Hoof, H. Friedrich, E.J. Hensen, J. Catal. 311 (2014) 88–101.
[42] E. Parry, J. Catal. 2 (1963) 371–379.
[43] G. Busca, Phys. Chem. Chem. Phys 1 (1999) 723–736.
[44] J.C. Védrine, A. Auroux, V. Bolis, P. Dejaifve, C. Naccache, P. Wierzchowski, E.G. Derouane, J.B. Nagy, J.-P. Gilson, J.H. van Hooff, J. Catal. 59 (1979) 248–262.
[45] N.Y. Topsøe, K. Pedersen, E.G. Derouane, J. Catal. 70 (1981) 41–52.
[46] J.M. Winfield, J. Fluorine Chem. 130 (2009) 1069–1079.
[47] M. Moreno, A. Rosas, J. Alcaraz, M. Hernández, S. Toppi, P. Da Costa, Appl. Catal. A 251 (2003) 369–383.
[48] G. Connell, J. Dumesic, J. Catal. 101 (1986) 103–113.
[49] G. Connell, J. Dumesic, J. Catal. 105 (1987) 285–298.
[50] N. Cardona-Martínez, J. Dumesic, J. Catal. 127 (1991) 706–718.
[51] T. Matsuda, H. Miura, K. Sugiyama, N. Ohno, S. Keino, A. Kaise, J. Chem. Soc., Faraday Trans. 75 (1979) 1513–1520.
[52] J.X. Chen, J.J. Zhou, R.J. Wang, J.Y. Zhang, Ind. Eng. Chem. Res. 48 (2009) 3802–3811.
[53] A. Ozaki, K. Kimura, J. Catal. 3 (1964) 395–405.
[54] K. Kimura, H. A-I, A. Ozaki, J. Catal. 18 (1970) 271–280.
[55] J.R. Sohn, A. Ozaki, J. Catal. 61 (1980) 29–38.
[56] T. Lehmann, T. Wolff, C. Hamel, P. Veit, B. Garke, A. Seidel-Morgenstern, Microporous Mesoporous Mater. 151 (2012) 113–125.
[57] X.J. Yao, T. Kong, S.H. Yu, L.L. Li, F.M. Yang, L. Dong, Appl. Surf. Sci. 402 (2017) 208–217.
[58] M.M. Feijen-Jeurissen, J.J. Jorna, B.E. Nieuwenhuys, G. Sinquin, C. Petit, J.-P. Hindermann, Catal. Today 54 (1999) 65–79.
[59] K. Teinz, S. Wuttke, F. Boerno, J. Eicher, E. Kemnitz, J. Catal. 282 (2011) 175–182.
[60] W. Mao, Y. Bai, W. Wang, B. Wang, Q. Xu, L. Shi, C. Li, J. Lu, ChemCatChem 9 (2017) 824–832.
[61] J.-W. Luo, J.-D. Song, W.-Z. Jia, Z.-Y. Pu, J.-Q. Lu, M.-F. Luo, Appl. Surf. Sci. 433 (2018) 904–913.
[62] C.A. Johnson, K.M. Thomas, Fuel 63 (1984) 1073–1080.
[63] I. Mochida, A. Uchino, H. Fujitsu, K. Takeshita, J. Catal. 51 (1978) 72–79.
[64] P. Van der Avert, B.M. Weckhuysen, Angew. Chem. Int. Ed. 41 (2002) 4730–4732.
[65] P. Van der Avert, B.M. Weckhuysen, Phys. Chem. Chem. Phys 6 (2004) 5256–5262.
[66] E. Milchert, W. Pazdzioch, J. Myszkowski, Ind. Eng. Chem. Res. 34 (1995) 2138–2141.
[67] B. Adamczyk, O. Boese, N. Weiher, S. Schroeder, E. Kemnitz, J. Fluorine Chem. 101 (2000) 239–246.
[68] W. Jia, L. Jin, Y. Wang, J. Lu, M. Luo, J. Ind. and Eng. Chem. 17 (2011) 615–620.
[69] P.M.C. Zapata, M.L. Parentis, E.E. Gonzo, N.A. Bonini, Appl. Catal., A 457 (2013) 26–33.
[70] M. Shirotori, S. Nishimura, K. Ebitani, Catal. Sci. Technol 4 (2014) 971–978.
[71] H. Bayahia, E.F. Kozhevnikova, I.V. Kozhevnikov, Appl. Catal. B 165 (2015) 253–259.
[72] B. Morrow, A. McFarlan, J. Non-Cryst. Solids 120 (1990) 61–71.
[73] J. Lavalley, Catal. Today 27 (1996) 377–401.